PHYSICAL REVIEW B VOLUME 55, NUMBER 23 15 JUNE 1997-I

# Luminescence in amorphous silicon *p-i-n* diodes under double-injection dispersive-transport-controlled recombination

Daxing Han, Keda Wang,* and Chenan Yeh
*Department of Physics and Astronomy, University of North Carolina at Chapel Hill, North Carolina 27599-3255*

Liyou Yang
*Solarex A Business Unit of Amoco/Enron Solar, Newtown, Pennsylvania 18940*

Xunming Deng
*Energy Conversion Devices, Incorporated, 1675 West Maple Road, Troy, Michigan 48084*

Bolko Von Roedern
*National Renewable Energy Laboratory, 1617 Cole Boulevard, Golden, Colorado 80401*
(Received 11 December 1996)

The temperature and electric-field dependence of the forward bias current and the electroluminescence (EL) in hydrogenated amorphous silicon ($a$-Si:H) $p$-$i$-$n$ and $n$-$i$-$p$ diodes have been studied. Both the current and the EL efficiency temperature dependence show three regions depending on either hopping-controlled or multiple-trapping or ballistic transport mechanisms. Comparing the thermalization-controlled geminate recombination processes of photoluminescence to the features of EL, the differences can be explained by transport-controlled nongeminate recombination in trap-rich materials. [S0163-1829(97)03624-2]

## I. INTRODUCTION

Photoluminescence (PL) has been well studied to explore the recombination processes and electronic properties of localized states in hydrogenated amorphous silicon ($a$-Si:H).[1–7] All of the features of PL such as the temperature dependence of the efficiency, the spectrum-peak-energy position and its temperature dependence, and the time dependence of PL, reflect the carrier distribution in the large density of localized tail states. A thermalization model[1,2,4] with an exponential band-tail density of states ($\exp[-E/kT_0]$) has been used to explain the features of the PL. At $T<50$ K the PL efficiency is near unity because there is no carrier thermalization, while at high excitation intensities a slight decrease with decreasing temperature was observed and explained by Auger recombination.[1,2] A broad featureless PL energy spectrum due to tail-to-tail radiative tunneling peaked at 1.3–1.4 eV was universally observed in device-quality $a$-Si:H samples. The PL efficiency is thermally quenched above 50 K. Generally, at room temperature, the PL efficiency is reduced by about four orders of magnitude and is hardly detectable. The temperature dependence of the PL efficiency is described by[4]

$$y_{\rm PL}=y_0\exp(-E_D/kT_0)=y_0\exp\left[-\left(\frac{T}{T_0}\right)\ln(\nu_0\tau_r)\right], \quad (1)$$

where $E_D=kT\ln(\nu_0\tau_r)$ is the demarcation energy, $\nu_0\cong10^{12}\ \mathrm{s}^{-1}$ is the attempt-to-escape frequency for excitation out of the trapping site, $k$ is the Boltzmann constant, and $\tau_r$ is the carrier radiative-recombination lifetime. Carriers which are trapped into states deeper than $E_D$ will have a high probability of radiative recombination, whereas carriers trapped into shallower states will be thermally excited to the mobility edge, and will either find other traps or diffuse away to a nonradiative center. The measured slope $T_L=T_0/\ln(\nu_0\tau_r)$ was found to be 20–25 K, by using an average lifetime $10^{4}$ s. One obtained $T_0\approx450-500$ K, i.e., a correct magnitude for the valence-band tail slope in $a$-Si:H. A widely distributed radiative-recombination lifetime peaked between $10^{-3}$ and $10^{-4}$ s has been found by transient PL studies at low temperatures.[2] The carrier lifetime reduced to $10^{-6}-10^{-7}$ s and appears to be controlled by nonradiative recombination at room temperature. Furthermore, the PL energy peak position $\mathrm{PL_{peak}}(T)$ shifts from 1.4 eV to 1.1 eV when the temperature increases from 50 to 250 K;[8] and the transient PL peak energy $\mathrm{PL_{peak}}(t)$ decreases from 1.45 to 1.3 eV when the measuring time changes from $10^{-8}$ to $10^{-2}$ s.[1,2,8] The temperature- and time-dependent shift of the PL peak energy can be described by the thermalization model as well as

$$\mathrm{PL_{peak}}(T)=\mathrm{PL_{peak}}(0)-kT\ln(\nu_0\tau_r), \quad (2a)$$

and

$$\mathrm{PL_{peak}}(t)=\mathrm{PL_{peak}}(0)-kT\ln(\nu_0 t). \quad (2b)$$

Under photoexcitation both PL and photoconductivity (PC) can be measured concomitantly. An anticorrelation of the temperature dependence of PC intensity and PL efficiency has been universally observed.[5,6] In addition, high electric fields are found to quench the PL and enhance the PC.[5,6] Thus, it appears as if the PL would arise from recombination of geminate $e$-$h$ pairs, whereas the carriers that escape geminate recombination could contribute to PC.

Alternatively, electroluminescence (EL) has been used to study localized states and recombination processes of the intrinsic layer in $a$-Si:H $p$-$i$-$n$ structures.[9–16] EL arises from

 © 1997 The American Physical Society

recombination of nongeminate $e$-$h$ pairs because the electron and hole are injected from opposite sides of the diode. In earlier EL studies,[13–16] other authors argued that the PL and EL were identical except for the low EL efficiency and the lower EL peak energy position. The latter was explained by optical interference effect.[14] The same researchers[14] suggested that the low EL efficiency is due to the fact that the recombination only takes place near the $p$-$i$ interface. Except for the geminate process in PL,[1–8] one would expect similar recombination processes in both EL and PL, i.e., regardless of the generation methods. However, significant differences in the features of EL and PL in the same $p$-$i$-$n$ or $n$-$i$-$p$ structures have been observed. The goal of this review paper is to present a model to explain the features of EL based on systematic experimental study.

We have explained[10] that the EL efficiency is as high as the PL efficiency, and that the recombination takes place within the whole $i$ layer because the carriers' lifetime is much longer than the transit time in conventional $a$-Si:H $p$-$i$-$n$ and $n$-$i$-$p$ diodes. In this work, we study the temperature and electric-field dependence, as well as the light-soaking effect on both forward current and EL comparing to PL in $a$-Si:H $p$-$i$-$n$ and $n$-$i$-$p$ structures. We explain the unique EL results by employing the concept of dispersive-transport-controlled nongeminate recombination in trap-rich semiconductors.[18]

## II. SAMPLE AND EXPERIMENTAL CONDITIONS

Device quality $a$-Si:H $p$-$i$-$n$ diodes were made on transparent-conducting-oxide (TCO) coated-glass and $n$-$i$-$p$ on TCO coated-stainless-steel substrates by plasma-enhanced chemical vapor deposition (PECVD), and $p$-$i$-$n$ diodes by photoenhanced CVD techniques. The TCO was textured to avoid interference fringes, except for one pair of 1.0-$\mu$m-thick identical samples deposited on both textured and smooth surfaces that were used to ensure that the structure of the EL spectrum is not due to optical interference effect. The top contacts were Ag, Al, or ZnO, the area was 0.1–0.3 cm$^2$. The $i$-layer thicknesses $L$ were 0.2, 0.3, 0.4, 0.5, 0.53, 0.55, 1.0, 1.1, 2.0, and 10.0 $\mu$m. Samples with $L \leq 0.55$ $\mu$m are called thin samples while $L \geq 1$ $\mu$m are called thick samples. Among them, the high performance $a$-Si:H $p$-$i$-$n$ solar cells were made by a dc glow discharge at Solarex.[11] The 0.5-$\mu$m intrinsic layers were made of either hydrogen-diluted silane or pure silane, denoted as $p$-$i_H$-$n$ and $p$-$i$-$n$, respectively. The sample preparation conditions and cell performance furnished by the fabricating laboratories are given elsewhere.[9–12]

States $A$ and $B$ denote the initial and the photodegraded state of the $p$-$i$-$n$ diode, respectively. The photodegraded state was reached by exposuring the sample to a 200-mW/cm$^2$ white light with a infrared-cutoff filter. From eight to one thousand hours light soaking through the glass side of the sample was used to reach state $B$.

An Ar-ion laser with output power of 0.25–3 W/cm$^2$ at 514.5 nm was used for PL excitation. The corresponding absorption depth is 800 Å in an undoped $a$-Si:H. For EL measurements, the applied voltage was obtained from a programmable pulse generator. The 10-Hz repetition rate with a 10-ms pulse width were typically used. We varied the forward bias current density between $10^{-4}$ and $10^2$ mA/cm$^2$. The contribution of thermal radiation to the signal was less than 2% of the total signal.[10] The EL efficiency temperature dependence was measured under a constant voltage condition. The sample temperature range was 30–350 K. The emitted photons were dispersed in a monochromator and detected by a liquid-nitrogen-cooled Ge detector through the glass side of the samples. A lock-in technique was used to collect the PL or EL luminescence signal. The response curve of the detector and the system optics were calibrated with a linear response detector.

## III. RESULTS

### A. The critical energies of carrier transport and recombination in trap-rich materials

In amorphous semiconductors, the continually distributed localized states affect the recombination processes as well as the transport. It is commonly accepted that the carrier transport in disordered materials is trap limited and it can be described by the so-called multiple-trapping (MT) model,[19,20] in which the carriers are frequently trapped in tail states and released by thermal excitation. In the MT model the carrier transport is considered to be taken place at the mobility band edge, and at certain times, the average trap energy of the carriers is given by the demarcation level $E_D$,

$$E_D = kT \ln(\nu_0 t), \quad \text{when } T < T_0, \tag{3}$$

$E_D$ is defined as the energy at which the thermalization rate $\nu_0$ is equal to the reciprocal of the observation time $t$ in the carrier transport measurement.[19,20] The deepest energy position of the demarcation energy $E_D$ is the bottom of the tail states, which is about 0.3–0.35 eV above $E_v$ and 0.1–0.15 eV below $E_c$ for the holes and electrons, respectively. The phonon-assisted transition rate (thermalization rate) $\nu_0 \approx 10^{12}$ s$^{-1}$ is greater than both the radiative- and nonradiative-recombination rate, $10^3-10^4$ and $10^6-10^7$ s$^{-1}$. The luminescence therefore occurs only after the majority of carriers have thermalized to a sufficiently low density of states that further phonon-assisted transitions are suppressed by the weak overlap to neighboring sites. The tail-to-tail luminescence peak energy reflects the carrier distribution in the tail states and is expected to have a time and temperature shift of the peak energy as shown in Eq. (2). The thermalization model is also used to explain the temperature dependence of the PL efficiency and to deduce the valence-band tail width by using the carrier's average lifetime $\tau_r$ instead of the observation time $t$ as shown in Eq. (1).

In the case of EL, we found that both the energy peak position $EL_{peak}$ and its temperature dependence do not follow the thermalization model, especially at low temperatures. We suggest that carrier transport has to be considered as an determining factor. The MT model provides a good description of the transport phenomena for temperature greater than ~200 K. At lower temperatures, the hopping transport in the exponential band tail (or through potential fluctuations) must be considered. The carrier transport then is no longer near the band edge $E_c$ ($E_v$) but at transport level $E_t$ that has been introduced by Monroe.[21]

$$E_t = kT_0 \ln(8/27R_0^3 N_0) - 3kT_0 \ln(T_0/T). \quad (4)$$

The first term is an energy which is estimated to be close to the mobility edge, so that the second term represent the shift of the transport path below $E_c$ (above $E_v$ for holes). Both hopping-up and hopping-down processes are permitted within band tails at about $T>200$ K, below this temperature only hopping transition to states of lower energy occur.[20] At about $T>200$ K the second term in Eq. (4) becomes very small, thus $E_t \approx E_c$ ($\approx E_v$ for holes) and the MT model is valid. When the band-tail distribution is broad (a greater $T_0$) and at low temperatures such that $T<T_0$ the electron-transport level shift below $E_c$ (above $E_v$ for holes) is most significant. Furthermore, in the dispersive regime ($T<200$ K for electrons, $T<350$ K for holes), it has been found that the carrier drift mobility increases as the field increases, in the same manner as it increases with increasing temperature.[22] In other words, the carriers transport level shifts towards the band edge with increasing of the electric field in that temperature range.

First we discuss the role of the critical energies $E_D(T)$ and $E_t(T)$ in the forward bias current. The steady-state forward current in $a$-Si:H $p$-$i$-$n$ and $n$-$i$-$p$ diode is a recombination limited current.[23,24] We discuss the applied-field range of $(2-10)\times 10^4$ V/cm in which both the recombination-rate and the current spatial distribution are uniform through the $i$ layer according to a numerical calculation.[25] Hence, one can obtain the properties of the $i$ layer from the measurements. The dominant factor that determines the forward current behavior is the conduction-band tail because the electrons move much faster than the holes. Thus, the forward current density is $J_F \cong J_n = \mu_n \tau_n E$.[26,27] One can obtain the electron-transport parameter, the mobility-lifetime product $\mu_n \tau_n(T)$, from the $J_F(T)$ curves. Figure 1(a) shows the calculated $E_D(T)$ and $E_t(T)$ positions as a function of temperature for electron according to Eqs. (2) and (3) by using $\nu_0 \tau_r = 10^5$ (with a nonradiative-recombination lifetime $\tau_r = 10^{-7}$ s) and $T_0 = 300$ K. The transport level $E_t(T)$ represents the balance of hopping and thermal excitation to $E_t(T)$; it shifts to the band edge as there is an increasing of temperature. The demarcation level $E_D(T)$, on the other hand, represents the balance of thermal excitation to the band edge and retrapping into the tail states; it shifts away from the band edge as there is an increasing of temperature. Considering the increase of the electric field in the same manner as an increase of temperature,[23] we calculated the transport levels, $E_t(T)$, at electric field equal to 2, 4, and 6, $\times 10^4$ V/cm. For a better fit to the experimental results of both the current and the luminescence, we consider the thermalization processes beginning at 80 K in the calculation. There are two transition temperatures, $T_{2e}$ and $T_{1e}$, in the figure. When $T<T_{2e}$, the transport energy level $E_t$ is deeper than the thermalization energy $E_D$, and electrons move along at $E_t$. The cross points of $E_t(T)$ and $E_D(T)$, $T_{2e} \approx 110$, 120, and 125 K, indicate the temperature where the carrier transport mechanism changes from a hopping-controlled to the MT regime where the electrons move still along $E_t$.[21] The other transition temperature $T_{1e} \approx 180$, 190, and 200 K, indicates the temperature where the transport energy level has reached the conduction-band edge $E_c$. Meanwhile, at a temperature of about $T_{1e}$ the electron de-

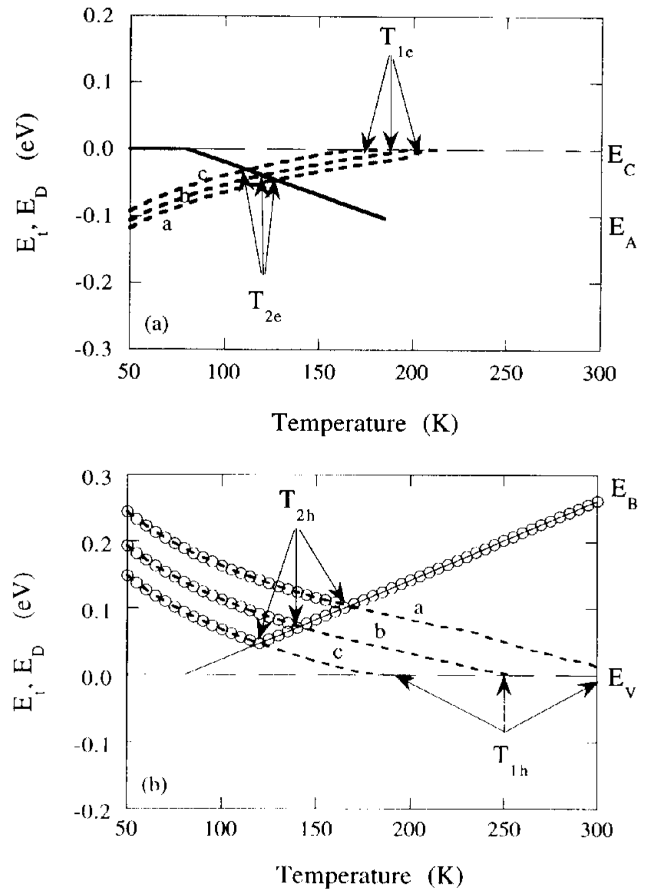


FIG. 1. (a) Calculated $E_t(T)$ and $E_D(T)$ positions as a function of temperature for electrons. $E_C$ and $E_A$ indicate the conduction-band edge and the bottom of the conduction-band tail, respectively. The solid line corresponds to $E_D = -kT \ln(\nu_0 \tau_r)$, and the dashed lines correspond to $E_t = -3kT_0 \ln(T_0/T)$, by using $\nu_0 \tau_r = 10^5$, $T_0 = 300$ K. The dashed lines $a$, $b$, and $c$ correspond to the electric field 2, 4, and $6\times 10^4$ V/cm, respectively. (b) Calculated $E_t(T)$ and $E_D(T)$ positions for holes as a function of temperature, $E_v$ and $E_B$ indicate the valence-band edge and the bottom of the valence-band tail, respectively. The solid line corresponds to $E_D = kT \ln(\nu_0 \tau_r)$, and the dashed lines correspond to $E_t = 3kT_0 \ln(T_0/T)$ by using $\nu_0 \tau_r = 10^6$, $T_0 = 450$ K. The open circles indicate the tunneling transition energy for $EL_{peak}$. The cross point of $E_t(T)$ and $E_D(T)$ indicate the temperature, $T_{2h}$, where the carrier transport mechanism changes. $T_{1h}$ indicates the temperature where the demarcation level has reached the bottom of the tail. The dashed lines $a$, $b$, and $c$ correspond to the electric field 2, 4, and $6\times 10^4$ V/cm.

marcation level $E_D$ has reached the bottom of the conduction tail $E_A$. When $T>T_{1e}$, the carriers move along the conduction-band edge; then the carrier transport can be described by ballistic model (free carriers drifting to a center) in steady-state measurements[23] while dispersive behaviors still can be seen in transient processes.[19-22,28]

We now discuss the role of the critical energies $E_D(T)$ and $E_t(T)$ in the EL. Because the valence-band tail is much broader than the conduction-band tail, the features of the EL is dominated by valence-band-tail states. According to Eqs. (2) and (3) by using $\nu_0 \tau_r = 10^8$ (with a radiative recombination lifetime $\tau_r = 10^{-4}$ s) and $T_0 = 450$ K for holes, Fig. 1(b)

shows the calculated demarcation energy and transport energy positions as a function of temperature and electric field for holes. At temperatures $T<T_{2h}$, the hopping-controlled regime determines the carriers transport. The transport level is deeper in the tail. If the $EL_{peak}$ is controlled by the transport level $E_t(T)$, rather than $E_D(T)$, the peak energy position of EL will be lower. $E_t(T)$ crosses $E_D(T)$ at temperature, $T_{2h}\approx 115$, 135, and 155 K, where $T_{2h}$ decreases with increasing electric field. The demarcation energy is deeper than the transport level in this regime, so the radiative tunneling occurs from $E_D$ with high probability and the EL energy peak position will be controlled by the demarcation energy. At $T_{1h}\approx 190$, 250, and 310 K the transport level reaches the valence-band edge $E_V$, causing the free carriers to be captured by deep states more efficiently.[23] Thus, recombination via defects will dominate.[10] Meanwhile, at a temperature of about $T_{1h}$ the hole demarcation level $E_D$ has reached the bottom of the valence tail $E_B$. This implies that the tail states are in thermal equilibrium with the band edge, thus the probability of the tail-to-tail radiative transition is very low. Consequently, one observes dominating defect EL for $T>T_{1h}$. We will see that the features of both the forward current and the EL temperature and electric-field dependence as well as the EL energy spectrum in $p$-$i$-$n$ structures can be explained by using the temperature dependence of the characteristic energy curves in Figs. 1(a) and 1(b).

### B. Forward bias current-temperature dependence

We show the forward current density $J_F$ temperature dependence data from the thin and thick $a$-Si:H $p$-$i$-$n$ and $n$-$i$-$p$ samples in their initial states $A$. Figures 2(a), 2(b), and 2(c) show the $J_F$ vs $1/T$ curves for a 0.5-$\mu$m $p$-$i_{\rm H}$-$n$ diode under a 2-, 3-, and 4-V bias, for a 0.5-$\mu$m $n$-$i$-$p$ diode at a 1.6-, 2.4-, and 4-V bias, and for a 2.0-$\mu$m $p$-$i$-$n$ diode under a 2–12-V bias, respectively. The electric field across the $i$ layer is $V_i/L=(V_a-V_{\rm bi})/L$, where $V_a$ is the applied voltage and $V_{\rm bi}=0.8$ V is the built-in potential. The general picture of the current-temperature dependence shows three regions corresponding to the three regions in Fig. 1(a):

(a) $T<T_{2e}$, the low-temperature hopping transport regime: the injected carriers move along the transport level $E_t$ that is deep down to the tail states as shown in Fig. 1(a). The weak temperature dependence of the current is due to a small activation energy of $\mu_n\tau_n$ which is about 0.01 eV, which is reasonable for the hopping activation energy.

(b) $T_{1e}<T<T_{2e}$, the MT regime: the transport level $E_t$ is above the demarcation level $E_D$. The carriers are still moving along at $E_t$ which is very close to $E_c$. The current is thermally activated with an activation energy which gives the activation energy of $\mu_n\tau_n$. In Fig. 2(a) one obtains the transition temperature $T_{2e}$ at 110–120 K which is consistent with the calculated curves in Fig. 1(a). For electric field 2, 4, and $6\times 10^4$ V/cm in the 0.5-$\mu$m $p$-$i$-$n$ diode, the activation energy is 0.08, 0.095, and 0.13 eV which agrees well with the results from electron drift mobility measurements.[21] In Fig. 2(b) the solid lines are from the $n$-$i$-$p$ diode while the dashed lines are from the same $p$-$i$-$n$ cell as in Fig. 2(a). One can see clearly that the transition temperatures of $T_{2e}$ and $T_{1e}$ shift to a higher temperature, which we believe is due to an injection limitation of the contact of the $n$-$i$-$p$

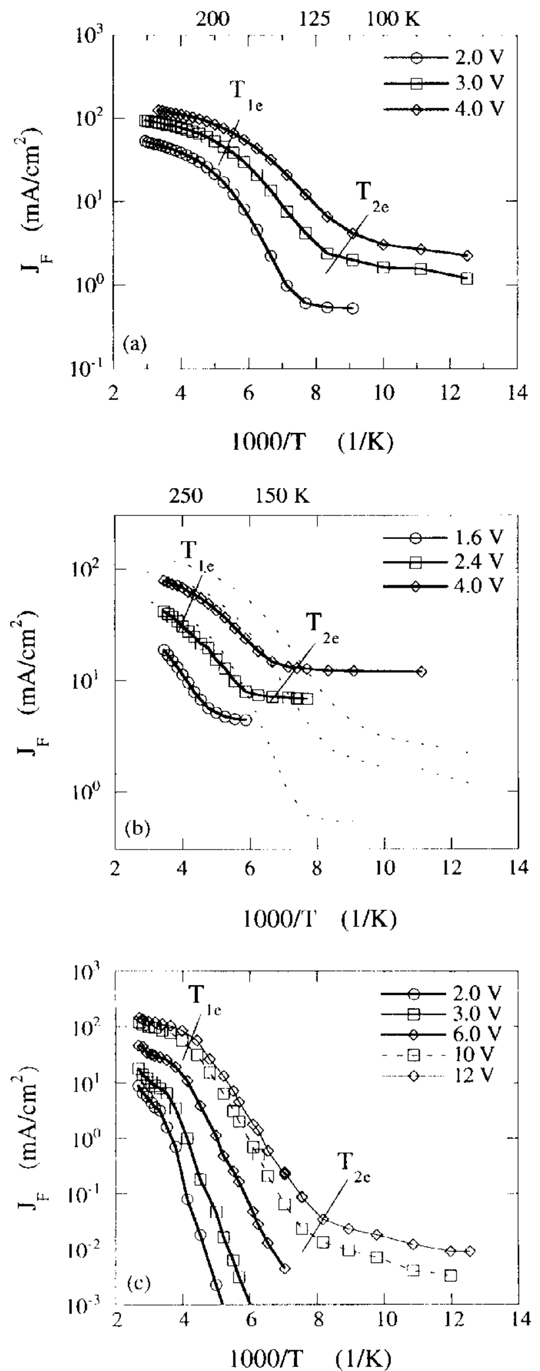


FIG. 2. Forward current density $J_F$ as a function of temperature from (a) 0.5 $\mu$m $p$-$i_{\rm H}$-$n$ diode under 2.0-, 3.0-, and 4.0-V bias; (b) 0.5-$\mu$m $n$-$i$-$p$ diode under 1.6, 2.4, and 4.0 V, the dashed lines from $p$-$i$-$n$ diode in (a); and (c) 2.0-$\mu$m $p$-$i$-$n$ diode under a 2-, 3-, 6-, 10-, and 12-V bias. Two transition temperatures $T_{1e}$ and $T_{2e}$ are indicated.

diode. A smaller activation energy 0.07–0.08 eV is obtained from the 0.5-$\mu$m $n$-$i$-$p$ than that from the 0.5-$\mu$m $p$-$i$-$n$ diode. An activation energy $\approx$0.07–0.15 eV was observed for the thin $p$-$i$-$n$ and $n$-$i$-$p$ diodes. The variation of the activation energy is due to the field dependence of the drift mobility. In Fig. 2(c), a larger activation energy of 0.2 eV is obtained for the 2.0-$\mu$m $p$-$i$-$n$ diode; perhaps, this thick sample made at an earlier time was not the best. The thick-

ness dependence of the drift mobility in this dispersive-transport regime may also play a role.[1,21]

(c) $T > T_{1e}$, the transport level $E_t$ has already reached the conduction-band edge $E_c$. The carrier transport is assumed to be of ballistic type,[23] thus the current is no longer thermally activated. However, the dispersive behavior still can be seen in transient measurements.[19-22,28] The calculated $T_{1e}$ is about 200 K in agreement with the experimental $T_{1e}$ in Figs. 2(a) and 2(b).

These three regions of forward current-temperature dependence are not always observed simultaneously in one curve. Under a low injection condition such as the 2.0-$\mu$m $p$-$i$-$n$ sample at 2–4-V bias shown in Fig. 2(c), one only observes a rapidly activated current range. This is due to the diffusion current increase with increasing temperature when the $J_F - V$ curves are in the diode region where the current increases exponentially with increasing bias voltage. At such low field the recombination rate profile in the $i$ layer is not uniform,[25] so one cannot deduce the $i$-layer properties from the $J_F$ vs $T$ curves. In contrast, for thin samples at a high applied field, one may only observe a weak temperature dependence of the current.[26] When the high field pushes $T_{1e}$ down to lower temperature close to $T_{2e}$, one would not observe the thermal activated regime of $T_{2e} < T < T_{1e}$.

### C. EL efficiency temperature dependence

The PL temperature dependence from the $p$-$i$-$n$ or $n$-$i$-$p$ structures follows the thermalization model described in Eq. (1) as the same as that from intrinsic films. However, carrier transport could play a role in the temperature dependence of EL. To measure the temperature dependence of the luminescence efficiency the generation rate should be kept constant. The generation rate of PL is simply proportional to the incident photon flux, but the generation rate of EL is more complicated. In early work,[13-16] the injected electron density $J_F/eL$ has been used as the generation rate. Consequently, constant current conditions were used to measure the EL efficiency temperature dependence in early EL work. We have suggested[9,10] the use a constant voltage instead constant current condition for the EL efficiency temperature-dependence measurements. Our previous studies[9,10] have explained that the generation rate of EL in $a$-Si:H diodes should be written as

$$g = (J_F/eL) \times (\tau_r/t_0) \cong J_F/e(\mu_n \tau_n E), \quad (5)$$

or

$$g = J_F/eL, \quad \text{when } (\tau_r/t_0) \leq 1,$$

where $J_F$ is the density of forward bias current, $\mu_n \tau_n$ is the electron mobility-lifetime product, $L$ is the thickness of the $i$ layer, and $t_0$ is the carrier transit time across the $i$ layer. $\mu_n \tau_n E = L_d$ (drift-length) should be used instead of the $i$-layer thickness $L$ in the expression of $J_F/eL$. The limitation for using $J_F/eL$ as the EL generation rate is $(\tau_r/t_0) \geq 1$, or $L_d/L \geq 1$. The carrier transit time is $t_0 = L^2/\mu_n V_i$. The electron transit time is about $2.5 \times 10^{-10}$ s with a band-edge mobility $\mu_n \cong 10$ cm$^2$/V s across a 0.5-$\mu$m-thick $i$ layer, under forward bias 1 V. The gain factor $\tau_r/t_0$ then is as large as $10^2 - 10^3$ when the electron recombination lifetime is $10^{-6} - 10^{-7}$ s. This explains that the early EL work found a $10^2 - 10^3$ times smaller EL efficiency than the PL efficiency, ignoring the gain factor $\tau_r/t_0$ in the generation rate expression, $g = J_F/eL(\tau_r/t_0)$. The hole lifetime is also longer than it's transit time if both the hole lifetime and the hole mobility are one order of magnetite lower than the electron's. Therefore, the injected electrons and holes must circulate through the diode before they find each other and recombine. The electrons circulate $10^2$ times more than the holes because of the higher mobility and the longer lifetime. So the carrier recombination take place through the whole $i$ layer indeed. The above argument about the gain factor will be valid in the temperature range $T > T_2$, where the MT model is valid; in other words, when the carrier transport takes place near the mobility edges. The carrier's mobility will decrease rapidly in the hopping transport regime when $T < T_2$,[21] and then the gain factors tend to be one.

The EL efficiency can be written as the total emission intensity per generation rate per unit area $A$,

$$y_{\text{EL}} = I_{\text{EL}}/\text{Ag} = (I_{\text{EL}}/I_F) \times e \mu_n \tau_n (V_i/L). \quad (6)$$

The total emission from the sample is $I_{\text{EL}}$, the forward current is $I_F = AJ_F$. Assuming that a small thermal activation energy of $\mu_n \tau_n$ product can be taken into account later, the factor $\mu_n \tau_n (V_i/L)$ does not change with temperature under constant voltage. Thus, $I_{\text{EL}}/I_F$ is the effective EL efficiency in temperature-dependence measurements *under a constant voltage condition*. In other words, a constant voltage (not a constant current) with a modification of the activation energy of $\mu_n \tau_n$ means a constant generation rate in the EL efficiency temperature-dependence measurements.

We show the experimental results of EL effective efficiency, $I_{\text{EL}}/I_F$, as a function of temperature for $p$-$i_{\text{H}}$-$n$ and $n$-$i$-$p$ samples with varied thickness in initial state $A$ in Fig. 3(a) for a 0.5-$\mu$m $p$-$i$-$n$ diode, in Fig. 3(b) for 0.3 and 0.5-$\mu$m $n$-$i$-$p$ diodes, and Fig. 3(c) for a 2.0-$\mu$m $p$-$i$-$n$ diode. Practically, as temperature increases the rapid increase of current density could breakdown the thin film diode, so we have only measured EL efficiency temperature dependence at temperatures near $T_{2h}$ (where the maximum efficiency is) for the 2.0-$\mu$m sample. Similar features of the $I_{\text{EL}}/I_F$ vs $T$ curves have been found from all the samples being measured. Interestingly, as temperature increases above 0 K there are three regimes in the $I_{\text{EL}}/I_F$ vs $T$ curves:

(a) $T < T_{2h}$, the efficiency $I_{\text{EL}}/I_F$ increases rapidly with temperature and depends on the applied voltage. The EL efficiency shows a maximum value at a transition temperature. $T_{2h}$ and the maximum efficiency vary with applied voltage and higher fields correspond to a lower $T_{2h}$ and higher efficiency.

(b) $T > T_{2h}$, the efficiency $I_{\text{EL}}/I_F$ decreases with temperature and does not depend on the applied voltage. It is reasonable that the $I_{\text{EL}}/I_F$ vs $T$ curves do not depend on voltage for $T > T_{2h}$, if the luminescence efficiency depends on the generation rate linearly.

(c) When $T$ is near room temperature, $I_{\text{EL}}/I_F$ does not change much with temperature due to the defect EL$_d$ domination. It is shown more clearly in Fig. 3(a) at $T > 250$ K. The enhancement of defect luminescence in EL comparing to PL will be discussed in Secs. III E and V B.

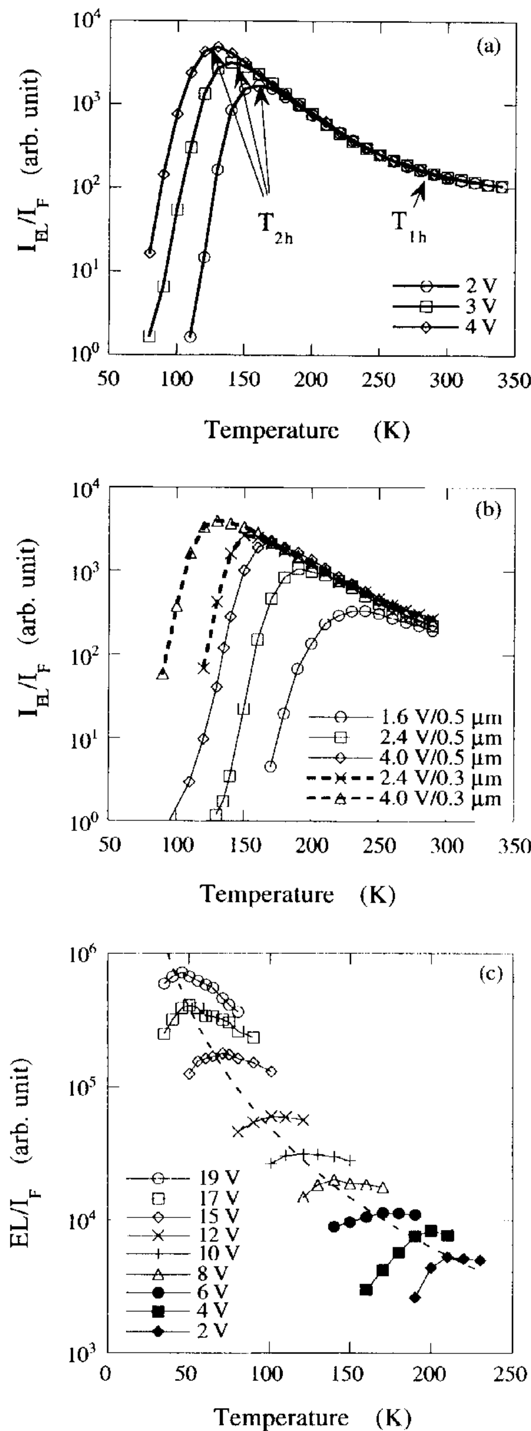


FIG. 3. EL effective efficiency $I_{EL}/I_F$ as a function of temperature for (a) 0.5-$\mu$m $p$-$i_H$-$n$ diode at a 2.0-, 3.0-, and 4.0-V bias; the transition temperatures $T_{2h}$ are indicated; (b) 0.3- and 0.5-$\mu$m $n$-$i$-$p$ diodes at a 1.6-, 2.4-, and 4-V bias; and (c) 2.0-$\mu$m $p$-$i$-$n$ diode at 2–19-V bias; the dashed line indicates $T_{2h}$ (see text).

We have mentioned above that the hole distribution in the valence-band tail is the dominant factor for the luminescence signal, and the tail-to-tail transitions dominate the integral EL efficiency at low temperatures. Thus, we explain the experimental results in Figs. 3(a), 3(b), and 3(c) by the calculated curves in Fig. 1(b) for holes. First, for $T<T_{2h}$ one expects the transport to be hopping controlled.[21,22] As the

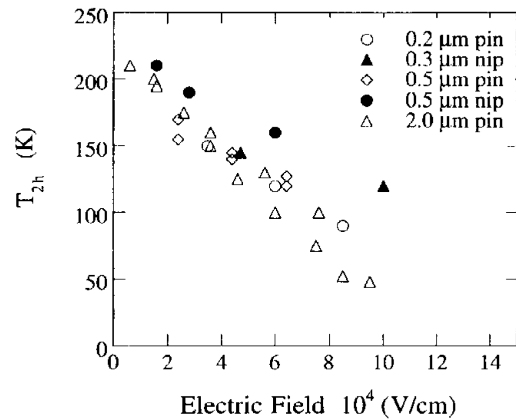


FIG. 4. $T_{2h}$ as a function of the electric field across the $i$ layer for 0.2-, 0.3-, 0.5-, and 2.0-$\mu$m $p$-$i$-$n$ and $n$-$i$-$p$ samples.

temperature decreases, the deeper is the transport level the less the wave functions overlap, hence the tunneling rate $\rho$ for the radiative recombination decreases exponentially according to $\rho=\nu_0\exp(-2R/R_0)$, where $R$ is the average electron-hole separation and $R_0$ is the effective Bohr radius.[1,29] It is worth mentioning here that this field-enhanced transition can only be seen in the case of nongeminate recombination.[29] An opposite situation occurs in geminate recombination processes such as the field quenching in PL.[5,6] It has been found that the carrier drift mobility increases as the field increases in the same manner as it increases with temperature.[22] In other words, the carriers move faster as the field increases. So one would predict that under a higher field the carrier transport would change to a MT regime at lower temperature. The EL efficiency temperature-dependence curves suggest that $T_{2h}\approx 125$, 135, and 150 K for applied voltage 2, 3, and 4 V, respectively, for the 0.5-$\mu$m $p$-$i_H$-$n$ diode of Fig. 3(a). In addition, as predicted by the calculated data in Figs. 1(a) and 1(b), for the same diode the transition temperatures for holes, $T_{1h}$ and $T_{2h}$ are both higher than $T_{1e}$ and $T_{2e}$ for electrons because of the much wider valence-band tail than conduction-band tail. This can be seen clearly in Figs. 2(a) and 3(a) for the same 0.5-$\mu$m $p$-$i_H$-$n$ diode, for instance, $T_{1h}$ and $T_{2h}$ at 2 V are both 150 and 250 K higher than $T_{1e}$ and $T_{2e}$ at about 120 and 220 K.

When $T>T_{2h}$, the EL effective efficiency $I_{EL}/I_F$ decreases with temperature similar to the PL efficiency that follows the thermalization model shown in Eq. (1). More details will be discussed in the following section.

It is clear that the transition temperature $T_{2h}$ depends on the applied field. In Fig. 4, we plot the $T_{2h}$ as a function of the electric field from a group of $a$-Si:H $p$-$i$-$n$ diodes including the data in Figs. 3(a), 3(b), and 3(c). One can see that the data show the reciprocal of the $T_{2h}$ proportional to the field, in good agreement with the field effect on the carrier dispersive transport.[1,21]

### D. Temperature and electric-field dependence of the EL energy peak position

It has been a puzzle why the EL peak energy has always been observed to be lower than PL peak energy of the same

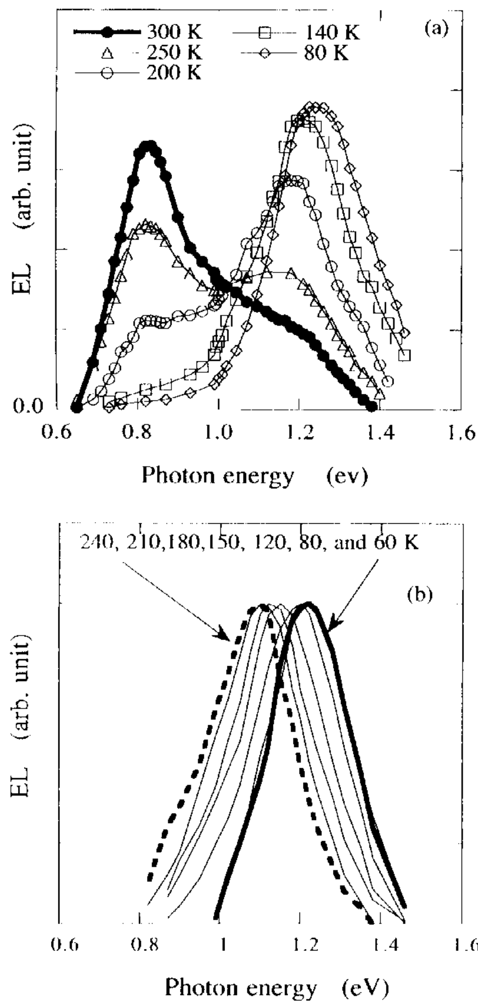


FIG. 5. EL spectrum temperature dependence from a (a) 0.2-$\mu$m and (b) 2.0-$\mu$m *a*-Si:H *p-i-n* diode.

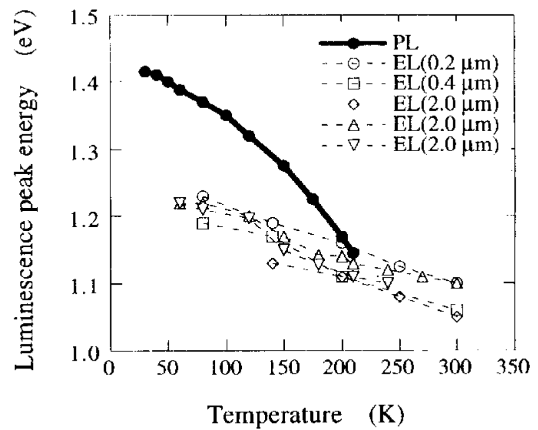


FIG. 6. Comparison of the luminescence peak energy as a function of temperature between $PL_{peak}$ and $EL_{peak}$ from 0.2-, 0.4-, and 2.0-$\mu$m *p-i-n* diodes.

sample.[9–17] We show the temperature dependence of the EL spectra at initial state *A* from both thin and thick *p-i-n* samples. In order to compare the spectrum line shape, the spectra were normalized to the same integral EL intensity. Figure 5(a) shows EL spectra from a 0.2-$\mu$m-thick *p-i-n* diodes, at a 2.5-V applied voltage. Both the main and the defect band can be seen clearly at $T>200$ K in thin samples. Figure 5(b) shows EL spectra from 2.0-$\mu$m-thick *p-i-n* diodes at a 20-V applied voltage. It is more like the PL spectra, the EL defect band is very weak in thick *p-i-n* samples. We notice that at low temperature in both thin and thick samples the EL main-band peak energy $EL_{peak}$ is about 1.2 eV. The EL spectrum temperature dependence was measured for several *p-i-n* diodes with varied *i*-layer thickness of 0.2, 0.4, 0.5, 0.53, 0.55, 1.0, 1.1, 2.0, and 10 $\mu$m at $(1-2)\times 10^4$ V/cm electric field. The features were similar, but the main band was relatively strong in thick samples with $L \leq 1$ $\mu$m, but the defect band was relatively strong in thin samples with $L \geq 0.55$ $\mu$m. This results in a thickness dependence of the EL spectrum line shape which contains both a main and defect band.[10]

In order to compare the main-band peak energies between EL and PL, the EL spectra were decomposed into two components.[30] Unlike the two-component EL spectrum, one can only observe the main-band PL from these high-quality intrinsic *a*-Si:H layers. In Fig. 6, we plot the main-band luminescence peak energy as a function of temperature for both $PL_{peak}$ and $EL_{peak}$ from 0.2, 0.4, and 2.0-$\mu$m *p-i-n* diodes. One can see that the $PL_{peak}(T)$ follows the thermalization model as described in Eq. (1), while the $EL_{peak}(T)$ does not. The PL spectra were measured by 0.1-W/cm$^2$ 514.5-nm laser excitation, and the EL spectra were measured under a $2\times 10^4$ V/cm applied field. It is clearly shown that the $EL_{peak}(T)$ temperature dependence is very weak in a wide temperature range of 50 to 300 K.

We have shown that the carrier transport plays a role in the features of the EL temperature dependence. The EL peak energy position also can be discussed according to the characteristic energies shown in Fig. 1(b). Since the carrier's hopping rate is much faster than the recombination rate, the carriers first hop down to their transport energy level and circle many times through the device then recombine from their transport levels. Therefore, when $T<T_{2h}$, the $EL_{peak}$ is controlled by the transport level $E_t(T)$ which is about 0.2 eV deeper than the energy position of $E_D(T)$ at low temperatures. As temperature increases, when $T>T_{2h}$ the energy position of $E_D(T)$ is lower than $E_t(T)$, the transition then occurs between the $E_D(T)$ with a higher probability. Thus $EL_{peak}$ will follow the thermalization model similar to that in PL. The open circles in Fig. 1(b) indicate the possible favorable transition energy for $EL_{peak}$. It shows a much weaker temperature dependence than that of $E_D(T)$. Therefore, $EL_{peak}(T)$ has weaker temperature dependence than $PL_{peak}(T)$. This is the case in Eq. (6). So both the lower EL peak energy position and its weaker temperature dependence are explained by dispersive-transport-controlled recombination.

More evidence of the dispersive-transport-controlled recombination is seen in the $EL_{peak}$ field dependence. At low temperature the $EL_{peak}$ shifts to a higher energy as the electrical field increases, as shown in Fig. 7 for a group of *p-i-n* samples at 100 K. A similar shift was observed at 90 and 140 K. However, we have not observed a shift of the $EL_{peak}$ with increasing electrical field at $T>200$ K. Again, the results agree with the field dependence of the carrier

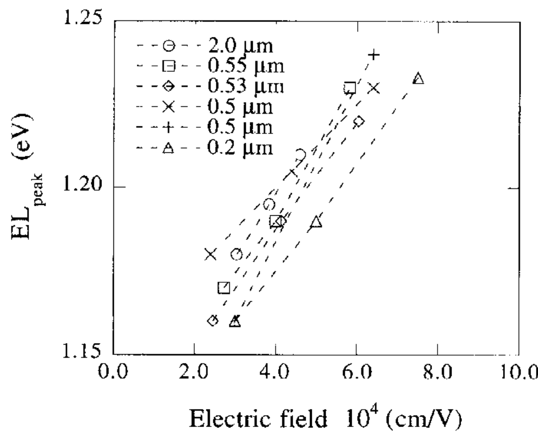


FIG. 7. $EL_{peak}$ as a function of the electrical field for 0.2-, 0.5-, 0.53-, 0.55-, and 2.0-$\mu$m *p-i-n* samples at 100 K.

dispersive transport.[22] That is, the higher the field the closer the transport level is to the mobility edge, so the higher the transition energy for the EL peak position in the dispersive-transport regime.

### E. Defect EL in *a*-Si:H *p-i-n* structures

We have seen in Fig. 5(a) that the defect luminescence intensity is relatively strong in thin *p-i-n* diodes. Now we discuss in more detail the defect luminescence in the MT regime. In Fig. 8 the EL efficiency, $EL/I_F$ vs $T$ data are plotted in comparison with the PL vs $T$ data for a group of *p-i-n* samples. The PL efficiency does not depend on the sample thickness but the EL does.[10] We found that the thermal quenching behavior of the EL efficiency, $I_{EL}/I_F$, in the *p-i-n* diodes can be divided into two groups depending on the *i*-layer thickness. For sample thicknesses greater than 1.0 $\mu$m, the lower group of curves in Fig. 8 shows a thermal quenching behavior of the EL efficiency which is similar to that of PL as described in Eq. (1); while the upper group of curves shows much less temperature dependence for sample thicknesses between 0.4 and 0.55 $\mu$m, which are typical for

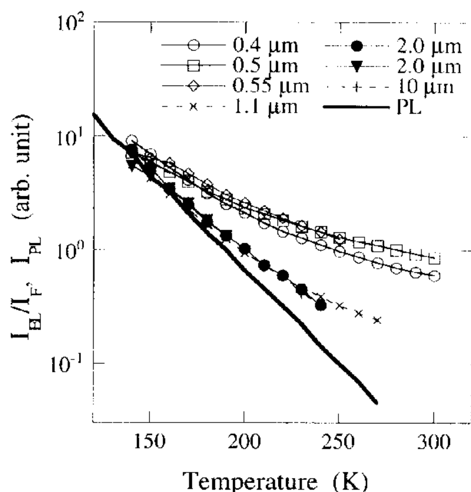


FIG. 8. EL effective EL efficiency, $EL/I_F$, vs temperature at $T>T_{2h}$ in comparison with the PL efficiency thermalization curve for a group of *p-i-n* samples.

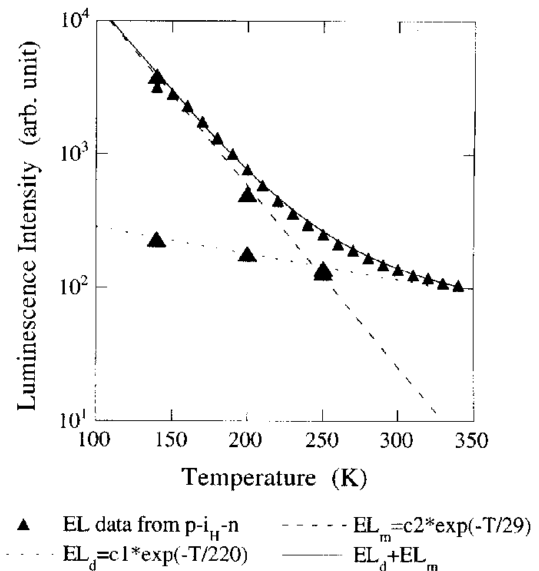


FIG. 9. EL efficiency at $T>T_{2h}$ from Fig. 8 for the 0.5-$\mu$m sample. The contributions from both the main-band $EL_m$ and the defect band $EL_d$ are indicated, respectively. The symbols of the solid and open triangles are the measured data from the 0.5-$\mu$m *p-i-n* cell. The dashed and solid lines show the best fit by using the functions expressed under the figure.

high-performance solar cells. Unfortunately, we do not have the samples with a thickness of 0.6–0.9 $\mu$m. One would expect that the data from such samples may fall into the region between these two groups.

In Fig. 9 we replot the data at $T>T_{2h}$ from Fig. 8 for the 0.5-$\mu$m sample. The EL photon energy spectra have been decomposed into two Gaussian bands at 140, 200, and 250 K: the 1.2-eV main band ($EL_m$), and the 0.85–0.9-eV defect band ($EL_d$).[10] The open circles and squares indicate the measured data of EL efficiency from a 0.5-$\mu$m *p-i-n* sample, and the solid circles, and triangles are the decomposed data for the main band $EL_m$, and the defect band $EL_d$. The defect band $EL_d$ shows a much weaker temperature dependence. The lines connecting $EL_m$ and PL are best fits according to Eq. (1) with slopes of 29 K for the main-band $EL_m$: The slope $T_L$ is found to be a sensitive parameter to characterize the quality of the *i* layer in a *p-i-n* structure. For instance, in a 0.5-$\mu$m *p*-$i_H$-*n* sample made with hydrogen dilution, we found $T_L=29$ K compared to 37 K for the non-H-diluted *p-i-n* sample shown in Fig. 8.[12] We obtain the slope in a range of $29<T_L<39$ K$^2$ of $I_{EL}/I_F$ vs $T$ curves, but $20<T_L<23$ K$^2$ for $I_{PL}$ vs $T$ curves in the same group of *p-i-n* samples. It is reasonable that the slope $T_L$ of $I_{EL}/I_F$ vs $T$ is larger than that of $I_{PL}$ vs $T$, because an activation energy of $\mu_n\tau_n$ product should be taken into account in the EL efficiency temperature-dependence measurements as shown in Eq. (7). The value of the activation energy can be obtained from the corresponding $J_F$ vs $T$ curves as shown in Fig. 2. It is in the range of 0.07–0.15 eV, depending on the field and sample thickness.

Because the defect luminescence signal is much stronger under double injection than under photoexcitation near room temperatures, one can use the EL spectrum to study the energy profile of the deep states in real *p-i-n* diodes. By com-

paring the EL defect spectra to the density of defect states deduced by transient-photocurrent measurements from the same group of samples, we were able to confirm that the defect luminescence band is due to radiative transition between defect and valence-band tail states.[12] We also have studied the photodegradation mechanism in *p-i-n* solar cells by using the defect EL spectroscopy.[12]

### F. Light-induced metastable effects

We have seen that the information of localized states, including both tail states and defect states, in the *i*-layer of the *p-i-n* or *n-i-p* diodes were obtained from the above forward current and EL temperature-dependence studies. In the above sections, we present the data of the original state *A*. The same measurements were done after light soaking. One of the light-induced changes in *a*-Si:H sample is the increase of the density of silicon dangling bonds (DB's) that reduces the carrier's recombination lifetime. DB's act as both radiative and nonradiative recombination centers. The defect band dominates the EL spectrum at room temperature. Light-induced metastable changes of the defect EL spectra reflect the metastable changes of the deep states.[11,12] As we have seen in Figs. 5(a) and 9, the defect electroluminescence intensity $EL_d$ is relatively strong in thin *p-i-n* diodes. Therefore, the light-induced degradation effect has been studied by defect EL spectroscopy, as reported previously.[12] Here we report the light-induced effects on the localized tail states as well as the dominating effects on carrier transport.

Figures 10(a) and 10(b) show the forward current density $J_F$ temperature dependence for 0.5-$\mu$m $p$-$i_H$-$n$ and *p-i-n* cells at state *B* after a 30-h light soaking. The dashed lines indicate the data from the same samples at initial state *A*. The light-induced effects are as follows:

(a) an increase of the current density at low-temperature hopping transport regime $T<T_{2e}$;

(b) an increase of the activation energy at $T_{1e}<T<T_{2e}$, which reflects an increase of the separation between $E_c$ and the bottom of the conduction-band tail $E_A$;

(c) no obvious change in the temperature range $T>T_{1e}$, where the carrier transport in steady-state is nondispersive.

The light-soaking effect on EL effective efficiency for the same group of cells before and after light soaking is shown in Figs. 11(a) and 11(b). Interestingly, there are no obvious changes of the EL effective efficiency upon light soaking in both the H-diluted and nondiluted samples when $T>T_{2h}$. This can be understood as the light-induced metastable change is contained in the transport parameter, $\mu_n\tau_n$, but does not show in the radiative-recombination processes. In previous work[10] we have shown that if the $\mu_n\tau_n$ product is included, i.e., $\mu_n\tau_n(A)\approx10^{-5}$ cm$^2$/V at state *A*, and $\mu_n\tau_n(B)\approx10^{-6}$ cm$^2$/V at state *B*, the EL efficiency shown in Eq. (6), $\mu_n\tau_n I_{EL}/J_F$, does decrease roughly an order of magnitude upon light soaking. The factor of $\mu_n\tau_n$ is excluded in the EL effective efficiency $I_{EL}/I_F$, so the light-induced effect cannot be seen in the temperature dependence in Fig. 11. When $T<T_{2h}$, the lower EL effective efficiency after light soaking could be related to the lower position of the transport level. This will be discussed more in the following.

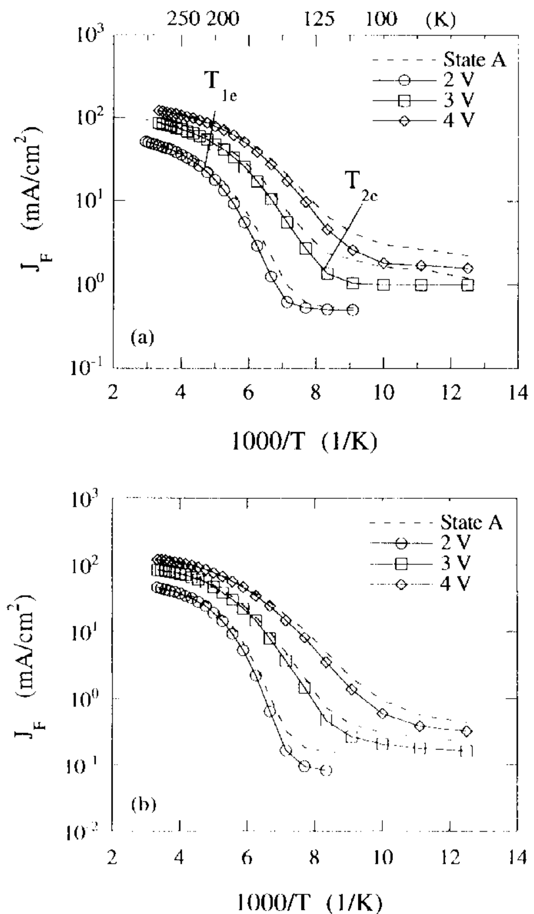


FIG. 10. Light-soaking effect on $J_F$ vs $1/T$ curves from 0.5-$\mu$m-thick (a) $p$-$i_H$-$n$ and (b) *p-i-n* cell at a 2.0-, 3.0-, and 4.0-V bias. The dashed lines correspond to the data at state *A*. Two transition temperatures $T_{1e}$ and $T_{2e}$ at state *A* are indicated in (a).

The main-band luminescence due to tail-to-tail transition dominates the EL spectrum at low temperatures. We observed a slight shift of the main-band peak energy position and a more pronounced low-energy shoulder after light soaking as shown in Fig. 12. The explanation for the lower EL peak energy position is that if the valence-band tail $T_0$ changes from 450–500 K, it will result as about 0.012 eV lower than the EL peak energy position according to the transport level as shown in Eq. (4). It is not too surprising that the valence-band tail is broadened upon light soaking if the conduction-band tail has also been broadened as shown from the current thermal activation curves in Figs. 10(a) and 10(b). In fact, in previous works[31,32] we have observed a light-induced increase of the Urbach tail width in intrinsic *a*-Si:H films by both a constant photoconductivity method and PL spectrum technique.

## IV. SUMMARY AND DISCUSSIONS

### A. Comparing EL to PL in *a*-Si:H

Temperature and electric-field dependence of a forward bias current and electroluminescence efficiency as well as their light-soaking effects in device-quality hydrogenated amorphous silicon *p-i-n* and *n-i-p* diodes have been studied. Both the current and the EL efficiency show three re-

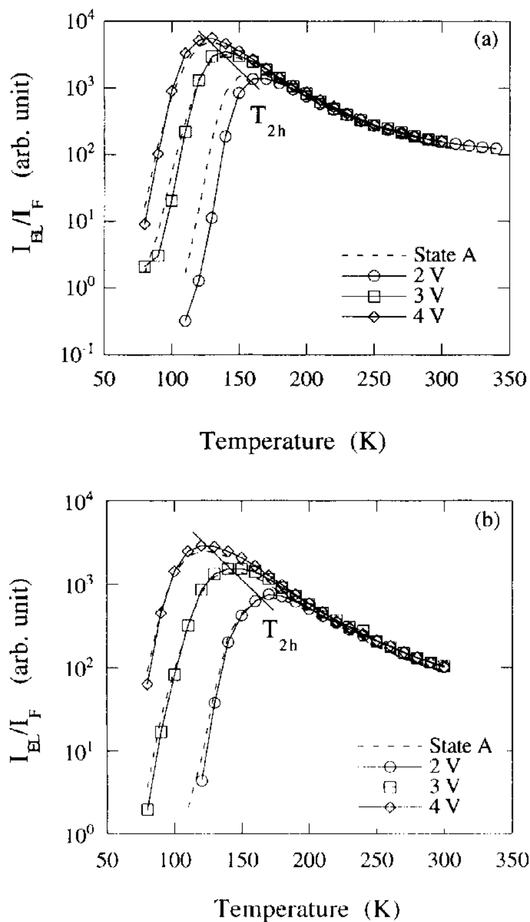


FIG. 11. Light-soaking effect on $I_{EL}/I_F$ vs $1/T$ curves from 0.5-$\mu$m (a) $p$-$i_H$-$n$ and (b) $p$-$i$-$n$ cell at 2.0-, 3.0-, and 4.0-V bias. The dashed lines correspond to the data at state $A$.

gions according to the transport mechanisms of either hopping controlled or multiple trapping, or ballistic (nondispersive). Compared to PL, significant differences in the features of EL were observed: (1) the EL main-band energy peak, $EL_{peak} \sim 1.2$ eV, is always 0.1–0.2 eV lower than the $PL_{peak}$; (2) the PL peak energy decreases with an increase of temperature, whereas the EL main-band peak energy hardly changes with temperature but changes with applied voltage; (3) at low temperatures, the PL intensity $I_{PL}$ is quenched but the $I_{EL}$ is enhanced by electric field; (4) the PL efficiency decreases with increasing temperature when $T > 50$ K, but the EL effective efficiency $I_{EL}/I_F$ increases rapidly with temperature and shows a maximum at a higher temperature $T_{2h}$ (100–200 K); finally; (5) the defect-band intensity is four orders of magnitude weaker than the main-band intensity in the case of PL at low temperatures whereas it is less than two orders of magnitude weaker in thin $p$-$i$-$n$ structures in the case of EL.

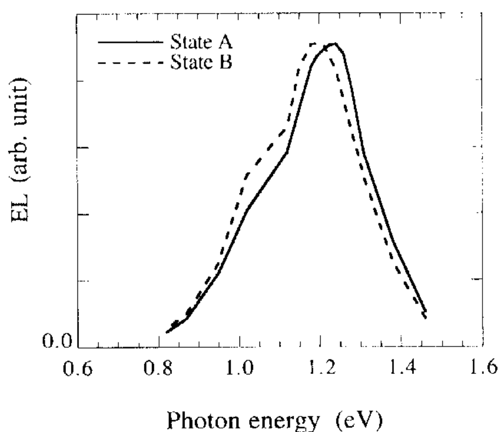


FIG. 12. EL spectra before and after light soaking from the same 0.5-$\mu$m $p$-$i$-$n$ cell as that in Figs. 10(b) and 11(b) at a 90-K, 4.0-V applied voltage.

In amorphous semiconductors the localized state distribution affects both the recombination processes and the transport. The main difference of the EL main band from PL is that the carrier transport is involved under a double injection. In the case of PL, the recombination is a thermalization-controlled geminate process whereas in the case of EL, the recombination is a dispersive-transport-controlled nongeminate process. However, when the demarcation energy is deeper than the transport level at $T > T_{2h}$, both the thermalization of the carriers in the valence-band-tail states and the transport processes are involved in EL. The origin of the temperature dependence of the transport parameter $\mu_n\tau_n(T)$ can be attributed to the thermalization of the electrons in the conduction-band-tail states. Therefore the features of both PL and EL intensity temperature dependence, $I_{EL}/I_F$, and $I_{PL}$ vs $T$ are similar as discussed in Fig. 9. If the temperature dependence of the transport parameter $\mu_n\tau_n(T)$ is taken into account, the width of the valence-band-tail $kT_0$ can be deduced from $(I_{EL}/I_F) \times \mu_n\tau_n(T)$ vs $T$ curve according to Eq. (1).

By employing the forward current and EL temperature-dependence studies information of both the localized tail states and the deep defect states in real solar cell structures were obtained concomitantly, which is crucial for the device performance. In thin $p$-$i$-$n$ diodes the defect EL intensity is two orders of magnitude stronger than that in the case of PL, so the room-temperature EL spectroscopy has been used to study photodegradation kinetics in solar cells.[12] One of the advantages of these studies, as compared to PL, is that the properties of the entire $i$ layer are obtained, because the recombination takes place through the whole $i$ layer in EL, but the PL signal is limited by the absorption depth of about 400–800 Å. The other advantages is that the low EL main-band peak energy due to dispersive-transport-controlled recombination allows us to explore the deeper tail states. In a previous studies[12] of the EL defect spectra in $p$-$i$-$n$ cells, we have reported that both the defect-state and tail-state energy distribution in the $i$ layer have been modified by hydrogen-dilution treatment. In this work, we show more evidence of the light-induced metastable increase of the $\mu_n\tau_n$ activation energy and the changes of the EL main-band spectrum line shape, that indicate a light-induced band-tail broaden, especially the deeper part of the tail states.

### B. Potential fluctuations

Another way of modeling the transport phenomena is to invoke long-range potential fluctuations.[33] In this picture, at low-temperature carriers can move in extended states, but

cannot always follow the electric field because of the potential fluctuations. At higher temperatures, the effective mobility becomes activated. In this picture too, one will find a shift of the transport path as discussed above as a function of electric field and free carrier density. Mobility measurements have directly shown such a field dependence of the mobility at room temperature.[34] The advantage of such a model is that one does not have to invoke limited temperature regimes for which a certain transport model will apply. Rather, the transport phenomena change gradually and continually, as the "randomness" with which the carriers can follow the applied electric field decreases with increasing temperature and field (movement of the effective transport level towards the band edge). However, to date no analytical description for such transport phenomena has been developed. At low temperatures, hopping models should be applicable, even though the carriers move through extended states, but are confined to "valleys" determined by the potential fluctuations.

### C. Defect EL

The threefold coordinated silicon DB is a defect in a fourfold-coordinated amorphous-silicon network, and is responsible for electronic states within the energy gap. These defect states are commonly assumed to play an essential role in determining transport and optoelectronic properties.[1] Despite both theoretical and experimental efforts, the nature of the DB still remains as one of the more controversial aspects of $a$-Si:H. One widely accepted model is that the DB's have a broad energy distribution in the gap, and they can be separated by their charge states into three classes: neutral, negatively charged, and positively charged defects, $D^0$, $D^-$, and $D^+$, respectively. There are four possible transitions for a defect with two gap states separated by a positive correlation energy $U$ as $e+D^0\rightarrow D^-$, $e+D^+\rightarrow D^0$, $h+D^-\rightarrow D^0$, and $h+D^0\rightarrow D^+$. We have clarified that the defect-to-valence band-tail transitions are responsible for the defect luminescence based on comparison studies of post-time-of-flight and EL spectroscopy.[12]

We now discuss the possible mechanism of the enhanced defect electroluminescence efficiency in thin $p$-$i$-$n$ diodes. In a thin diode the whole $i$ layer is depleted, thus the dangling bonds are charged as $D^-$ and $D^+$ near the $n$-$i$ side and the $p$-$i$ side. If the $D^-$ and $D^+$ have a high probability for radiative transition, one will obtain enhanced defect EL signals in thin $p$-$i$-$n$ cells. We obtained that the defect $EL_d$ band dominates the EL spectrum under a low applied voltage, such as 0.8 V for the 0.4–0.5-$\mu$m $p$-$i$-$n$ cells. As the applied voltage increases, most of the injected carriers are trapped in the tail states and there is a built-up positive space charge near the $p$-$i$ side, and a negative space charge near the $n$-$i$ side while the DB's are still in charged states. Since the $h+D^-\rightarrow D^0$ transition is radiative, more portions of charged dangling-bond states in the thin $i$ layer will enhance the radiative transition. Following a radiative transition $h+D^-\rightarrow D^0$, the $D^0$ can transfer back to $D^-$ by a charge depletion process, $D^{0e}\rightarrow D^-$ (electron diffuses from $n$ layer to $i$ layer) before the injected electron is captured by the nonradiative center $D^0$. So the charge depletion not only enhances the radiative transition $h+D^-\rightarrow D^0$ but also depresses the nonradiative transition $e+D^0\rightarrow D^-$. On the other hand, for the thick 2–10-$\mu$m $p$-$i$-$n$ samples, a great part of the $i$ layer is not depleted, and the defect recombination is dominated by nonradiative recombination via $D^0$. The charge depletion also does not occur in the PL process under photoexcitation. Therefore, there is no enhancement of the defect radiative transitions in both EL from thick samples or in PL. Consequently, the efficiency temperature dependence of the total EL from thick samples is similar to the PL as shown in Fig. 8.


### ACKNOWLEDGMENTS

The work of D. Han, K. Wang, and C. Yeh was supported by the National Renewable Energy Laboratory (NREL) under Subcontract No. XAN-4-13318-09. L. Yang would like to thank NREL for support under Subcontract No. RAN-4-13381-01. X. Deng would like also to thank NREL for support under Subcontract No. ZAN-4-13318-11. B. Von Roedern acknowledges support from the U.S. Department of Energy under Contract No. DE-AC36-83CH10093. We like to thank the $a$-Si group at NREL, and the Institute for Energy Conversion at the University of Delaware for providing samples. We thank F. Rubinelli and S. Fonash at Pennsylvania State University for the numerical calculations. Four sets of EL data were taken at Dr. R. Carius's laboratory, Julich, Germany, when D.H. and K.W. visited his laboratory. We also acknowledge helpful discussions with Dr. R. Carius.


*Present address: March Instruments, Inc., Concord, CA 94520.


[1] R. A. Street, *Hydrogenated Amorphous Silicon* (Cambridge University Press, Cambridge, 1991), Chaps. 4, 6–8.

[2] R. A. Street, Adv. Phys. **30**, 593 (1981); in *Hydrogenated Amorphous Silicon*, edited by J. Pankove, Semiconductors and Semimetals, Vol. 21B (Academic, Orlando, 1984), p. 197.

[3] D. J. Dunstan and F. Boulitrop, Phys. Rev. B **30**, 5945 (1984).

[4] R. W. Collins, M. A. Paesler, and W. Paul, Solid State Commun. **34**, 833 (1980); R. W. Collins and William Paul, Phys. Rev. B **25**, 5257 (1982).

[5] K. Jahn, R. Carius, and W. Fuhs, J. Non-Cryst. Solids, **97/98**, 575 (1987).

[6] W. Fuhs and K. Jahn, in *Amorphous Silicon and Related Material*, edited by H. Fritzsche (World Scientific, Singapore, 1988), pp. 767–778.

[7] B. I. Shklovskii, H. Fritzsche, and S. D. Baranovskii, Phys. Rev. Lett. **62**, 2989 (1989).

[8] C. C. Tsai and R. A. Street, Phys. Rev. B **19**, 2041 (1979).

[9] Keda Wang, Daxing Han, M. Kemp, and M. Silver, J. Non-Cryst. Solids **137&138**, 599 (1991).

[10] Daxing Han and Keda Wang, J. Non-Cryst. Solids **190**, 74 (1995).

[11] Keda Wang, Daxing Han, M. Kemp, and M. Silver, Appl. Phys. Lett. **62**, 157 (1993).

[12] Daxing Han, Keda Wang, and Liyou Yang, J. Appl. Phys. **80**, 2475 (1996).

[13] J. I. Pankove and D. E. Carlson, Appl. Phys. Lett. **29**, 620 (1976).

[14] T. S. Nashashibi, I. G. Austin, T. M. Searle, R. A. Gibson, W. E. Spear, and P. G. Le Comber, Philos. Mag. B **45**, 553 (1982).

[15] R. Carius, *Amorphous Silicon Technology*—1990, edited by E.

A. Schiff, M. J. Thompson, A. Madan, K. Tanaka, and P. G. LeComber, MRS Symposia Proceedings No. 192 (Materials Research Society, Pittsburgh, PA, 1990), pp. 101–106.

[16] T. M. Searle, M. Hopkinson, W. A. Jackson, A. J. Rhodes, and G. K. Diprose, Philos. Mag. B **63**, 179 (1991).

[17] C. Yeh, Daxing Han, Keda Wang, and L. E. McNeil, in *Amorphous Silicon Technology*, edited by E. A. Schiff, M. Hack, A. Madan, and A. Matsuda, MRS Symposia Proceedings No. 377 (Materials Research Society, Pittsburgh, 1995), pp. 281–286.

[18] Daxing Han, Keda Wang, and Bolko Von Roedern, Phys. Rev. Lett. **77**, 4410 (1996).

[19] T. Ticje and A. Rose, Solid State Commun. **37**, 49 (1980).

[20] J. Orenstein and M. Kastner, Phys. Rev. Lett. **46**, 1421 (1981).

[21] Don Monroe, Phys. Rev. Lett. **54**, 146 (1985).

[22] J. M. Marshall, R. A. Street, and M. J. Thompson, Philos. Mag. B **54**, 51 (1986).

[23] M. E. Zvanut, D. Han, K. Wang, and M. Silver, *Amorphous Silicon Technology—1990*, edited by P. C. Taylor, M. J. Thompson, P. G. LeComber, Y. Hamakawa, and A. Madan, MRS Symposia Proceeding No. 192 (Materials Research Society, Pittsburgh, 1990), pp. 305–309.

[24] Daxing Han, Keda Wang, and M. Silver, J. Non-Cryst. Solids **164–166**, 339 (1993).

[25] The numerical calculations were done by F. Rubinelli at S. Fonish's laboratory University Penn by using AMPS.

[26] Keda Wang, M. Silver, and Daxing Han, J. Appl. Phys. **73**, 4567 (1993).

[27] M. Hack and R. A. Street, J. Appl. Phys. **72**, 2331 (1992).

[28] Daxing Han, Douglas C. Mecher, E. Schiff, and M. Silver, Phys. Rev. B. **48**, 8658 (1993).

[29] Daxing Han and Keda Wang, Appl. Phys. Lett. **66**, 879 (1995).

[30] Keda Wang, Daxing Han, and M. Silver, in *Amorphous Silicon Technology—1994*, edited by E. A. Schiff, M. Hack, A. Madan, M. Powell, A. Matsuda, MRS Symposia Proceedings No. 336 (Materials Research Society, Pittsburgh, 1994), pp. 861–866.

[31] Daxing Han, Changhua Qiu, and Wenhao Wu, Philos. Mag. B **54**, L9 (1986).

[32] Daxing Han, M. Yoshida, and K. Morigaki, J. Non-Cryst. Solids **97/98**, 651 (1987).

[33] B. Von Roedern, Appl. Phys. Commun. **13**, 177 (1994).

[34] Y. Tang, S. Dong, R. Braunstein, and B. Von Roedern, Appl. Phys. Lett. **68**, 640 (1996).